Check for updates

Evaluating Maxwellian view design with a non-equal weighting matrix

Fenglin Xi, Xiayu Feng*, Philip Bos**
***Liquid Crystal Institute, Kent State University, Kent, OH, 44240, USA**

Abstract

In this work, we proposed an algorithm to evaluate any reflective polarization volume hologram (R-PVH) Maxwellian view design based on a non-equal weighting matrix of the field of view and gaze angle. A continuous eye movement from 0 to 17 degrees towards the ear is considered. The comparison of the eyebox of the example designs is presented after using the weighting matrix of the field of view and gaze angle. This algorithm gives us a method to evaluate any design based on the weighted distance to the center of the pupil.

Author Keywords

Maxwellian system; Polarization sensitive combiner; Augmented reality

1. Introduction to the aberration at the pupil in a reflective Maxwellian AR system

A Maxwellian view system uses a combiner to converge rays from different locations in the field of view (FOV) to the center of the pupil. In an example system described by Lee et al.[1], a point source is used as the ray generator. The individual rays are then modulated with FOV information converged to the center of the pupil, as shown in figure 1. However, in the figure, the ray amplitude modulator is not shown.

We can find the grating vector field $\vec{k}_{grating}(\vec{S},\vec{P},\vec{C})$of the combiner given the on Bragg source location $\vec{S}$=(S_x, S_y, S_z), the center of the pupil $\vec{P}$=(P_x, P_y, P_z), and the grating point location on the combiner $\vec{C}$=(C_x, C_y, C_z).

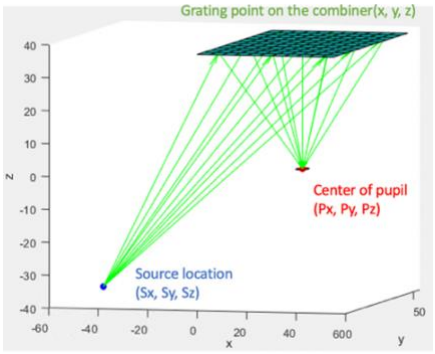

Figure 1. (a) For the unrotated eye, the grating vector field is designed to be on Bragg condition for deflected rays entering the eye at the center of the pupil. (b)View at the pupil plane.

The grating vector $\vec{k}_{grating}(\vec{S},\vec{P},\vec{C})$ on the combiner is defined using Bragg condition incident and deflect wave vector in grating $\vec{k}_{in}(\vec{S},\vec{r})$ and $\vec{k}_{def}(\vec{P},\vec{C})$ for any point on the combiner(C_x, C_y, C_z), so that rays from the source location a specified location (S_x, S_y, S_z) will be precisely deflected to a defined location of the pupil (P_x, P_y, P_z).

$$kx_{grating}(\vec{S},\vec{P},\vec{C}) = kx_{def}(\vec{P},\vec{C}) - kx_{in}(\vec{S},\vec{C}) \quad (1)$$

$$ky_{grating}(\vec{S},\vec{P},\vec{C}) = ky_{def}(\vec{P},\vec{C}) - ky_{in}(\vec{S},\vec{C}) \quad (2)$$

$$kz_{grating}(\vec{S},\vec{P},\vec{C}) = kz_{def}(\vec{P},\vec{C}) - kz_{in}(\vec{S},\vec{C}) \quad (3)$$

When the eye rotates, not all deflected rays will enter the center of the pupil. To steer the ray back to the center of gaze of the rotated pupil, [1] shows that moving the source point in the vertical direction is the best approach for steering the focus point of the rays to the point of the center of the rotated pupil. As shown in [1], while it is possible to direct the deflected beam from the center of gaze to the center of the pupil at its new location, the other rays no longer enter the center of the pupil. This limited eye box causes image aberrations.

2. The approach

There are two main approaches to increasing the eyebox of the Maxwellian view combiner. One of the approaches is eyebox replication. Multiple viewpoints can be achieved by either using two Pancharatnam-Berry deflectors (PBDs) [2] by Lin et al.&[3] by Wang et al., Dammann grating [4] by He et al., or Lens-Array-Based Holographic Optical Element[5] by Xia et al.

Although the eyebox is expanded, multiple viewpoints indicate the efficiency drops accordingly. Also, the double image problem is observed between different viewpoints shown in [6] by Kim et al.

Pupil steering is another solution to increase the eyebox in the Maxwellian view system without decreasing the efficiency and causing a double image. In [7] by Jang et al., a dynamic eyebox is achieved by changing the incident angle of the parallel rays design in a reflective transparent holographic image combiner (HIC). In [8], Xiong et al. use a stack of Cholesteric liquid crystal layers of opposite handiness and a half-wave retarder. From the cholesteric liquid crystal's polarization selectivity, two viewpoints are achieved in the example. More viewpoints are considered to be added by stacking more layers of cholesteric LC and active polarization converters, but the approach does not provide for a continuously variable gaze angle.

The main issue of the design in [8] is that a layer and a polarization controller need to be added for many gaze angles. This will cause increased complexity and weight of the head-worn combiner. But also, it is considered that the eye has several fixed gaze angles. It is rather desired that the optical system continuously follow the gaze angle of the eye. In previous studies, the deflected beam from different FOV is considered equally in [9] by Li et al. However, this would lead to a non-ideal design, as the resolution of the human retina is much higher near the center of gaze.

A Maxwellian system similar to [10] by Zou et al. is evaluated in this work as an example design. In the evaluated Maxwellian zone design, the bottom layer has one zone while the top layer has two zones. As in [10], the basic idea is to use two layers that reflect circularly polarized light with the opposite handiness. When the gaze angle is between [-θ, θ], the polarization state of the incident beam will be the one reflected by the first layer, whose grating vector field is "on Bragg" for the unrotated eye. When the gaze angle is larger than θ, the polarization state of the incident beam is changed to the orthogonal polarization state that will be unaffected by the first layer but reflected by the second layer, whose grating vector field is "on Bragg" for a gaze angle= α. This way, compared with a single layer, the grating vector used for the deflected beam is closer to the required grating vectors for each gaze angle.

The Bragg condition for the first layer is when the source is at $\vec{S_0}$=(S_{x_0}, S_{y_0}, S_{z_0}) and the deflected beam goes to the center of the unrotated eye(gaze angle =0 degree) at $\vec{P_0}$ =(P_{x_0}, P_{y_0}, P_{z_0}) for LHC incident. According to (1) to (3), the grating vector field for the first layer is $\vec{k}_{grating}(\vec{S_0}, \vec{P_0}, \vec{C})$.

The Bragg condition for the left part of the second layer is when the source is at $\vec{S_\alpha}$=($S_{x_+\alpha}$, $S_{y_+\alpha}$, $S_{z_+\alpha}$) and the deflected beam goes to the center of the α degree rotated eye(gaze angle = α degree) at $\vec{P_\alpha}$=($P_{x_+\alpha}$, $P_{y_+\alpha}$, $P_{z_+\alpha}$) for RHC incident. The Bragg condition for the right part of the second layer is when the source is at $\vec{S_{-\alpha}}$=($S_{x_-\alpha}$, $S_{y_-\alpha}$, $S_{z_-\alpha}$) and the deflected beam goes to the center of the -α degree rotated eye(gaze angle =-α degree) at $\vec{P_\alpha}$=($P_{x_-\alpha}$, $P_{y_-\alpha}$, $P_{z_-\alpha}$)for RHC incident.

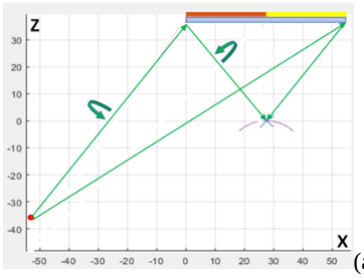

(a)

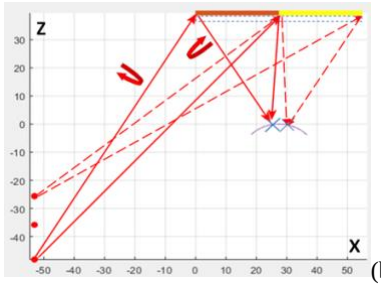

(b)

Figure 2. (a)The solid line indicates the Bragg condition for the first layer. The dot is the source location $\vec{S_0}$, and the cross is the center of the 0-degree rotated eye $\vec{P_0}$. (b)Solid lines indicate the Bragg condition for the second layer left half. The upper dot is the source location $\vec{S_\alpha}$ and the left cross is the center of the α degree rotated eye $\vec{P_\alpha}$. Dashed lines indicate Bragg condition for the second layer right half. The lower dot is the source location $\vec{S_{-\alpha}}$ and the right cross is the center of the –α degree rotated eye $\vec{P_{-\alpha}}$.

According to (1) to (3), the grating vector field for the left part of the second layer is $\vec{k}_{grating}\left(\vec{S_\alpha}, \vec{P_\alpha}, \vec{C}\right)$. The grating vector field for the right part of the second layer is $\vec{k}_{grating}\left(\vec{S_{-\alpha}}, \vec{P_{-\alpha}}, \vec{C}\right)$.

3. Method to find the interception point of the deflector wave vector and the pupil plane

In this section, the performance of the example design is analyzed. The main issue here is that when the gaze angle of the eye does not correspond to pupil locations of $\vec{P_0}$, $\vec{P_\alpha}$, $\vec{P_{-\alpha}}$, the rays from the combiner are not expected to all converge at the center of the pupil.

In this analysis, the location of the point light source is chosen to steer the ray from the combiner at the center of gaze (for the pupil location) to be directed to the center of the pupil. Then the intersection points of rays corresponding to different points in the field of view, with the plane of the pupil, will be found. A single metric number is determined by considering the weighted distance of the ray intersection points to the center of the pupil.

First, the wave vectors of rays reflected by the combiner for a given point source location are found, and then the intersection points with the plane of the pupil.

The point source location is chosen to cause light from the center of gaze to enter the center of the pupil, and then with that source location, the wave vectors for the remainder of the rays are found.

From the conservation of the tangential components of the incident, deflected and grating k vectors, we can find the tangential components of off Brag condition incident and deflect wave vector in grating $\vec{k}_{in}'(\vec{S}, \vec{r})$ and $\vec{k}_{def}'\left(\vec{P}, \vec{C}\right)$. Normal component of $\vec{k}_{in}'(\vec{S}, \vec{r})$ and $\vec{k}_{def}'\left(\vec{P}, \vec{C}\right)$ can be found by normalization condition.

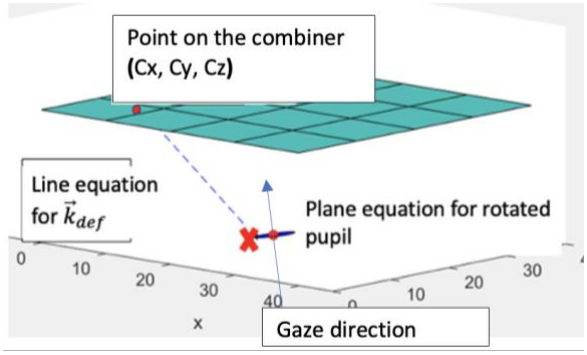

Figure 3. Interception point between the deflected beam and the pupil plane

As shown in Figure 3, the plane of the rotated pupil can be defined by a point(center of the pupil) and a normal vector (the gaze direction). The line equation of the deflected beam can be determined by a point(grating point on the combiner(Cx, Cy, Cz) and a vector($\vec{k}_{def}'\left(\vec{P}, \vec{C}\right)$) .

4. Method to evaluate the interception point:

21680159, 2023, 1, Downloaded from https://sid.onlinelibrary.wiley.com/doi/10.1002/sdtp.16844 by Kent State University Standing Orders, Wiley Online Library on [03/06/2024]. See the Terms and Conditions (https://onlinelibrary.wiley.com/terms-and-conditions) on Wiley Online Library for rules of use; OA articles are governed by the applicable Creative Commons License

weighted distance from the interception point to the center of the pupil

To quantitively describe the combiner performance, the distance from the interception points to the center of the rotated eye is weighted for each FOV. The "weight" of the distance of a ray corresponding to a particular field of view angle is determined by the eye's resolution ability for that angle. This is done because rays entering the pupil from the center of gaze will intercept the foveal region of the retina. In contrast, light entering the pupil at a large angle will intercept the retina, where there is a much lower density of receptors. The weighting coefficients chosen are derived from a paper by Chang et al. [11], which reports the eye's imaging ability vs. field of view.

FOV of +-2.5°,+-10°,+-20°, and +-30° is shown as a cross, asterisk, plus sign, and circle. Their FOV weighting coefficient is 250,15,10 and 5.

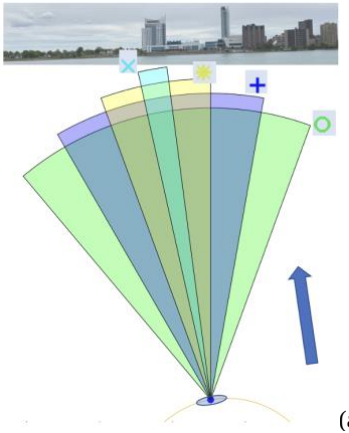

(a)

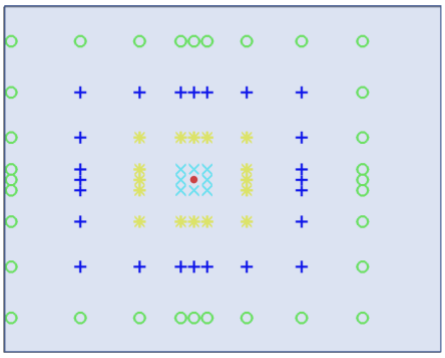

(b)

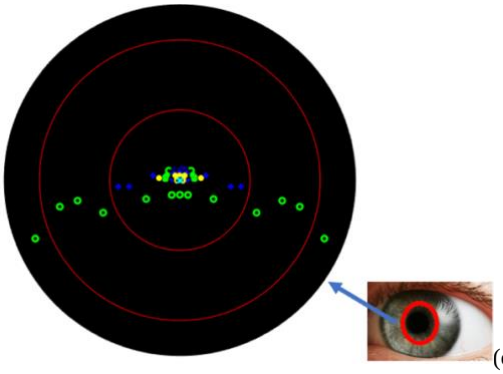

(c)

Figure 4. (a)Different markers indicate different FOV. (b)The front view of the combiner and FOV points is represented by different shapes(c)Top view of the pupil plane. The inner and outer circle has a 1mm and 2mm radius. The filled circle has a radius of 2.5mm. The dots are the interception points between the deflected beam and the pupil plane. The shape of the dot is an indication of the FOV location it corresponds to.

For a specific gaze angle, we have,

$$V_{gazeangle} = \sum_{FOV} D_{FOV} * W_{FOV} \quad (4)$$

$V_{gazeangle}$ is the weighted distance between the interception points to the center of the pupil for a specific gaze angle. D_{FOV} is the average distance of a specific FOV interception point to the center of the eye.

Because the center of gaze(FOV=0 degree) is the most important FOV point, for any gaze angle, we always choose the source location that steers the deflected beam from the center of gaze to the center of the rotated pupil, as described in section 3.

When looking at an object, we are more likely to gaze right at it than to gaze at it at a large angle. This means we also should weigh the distance between the interception point to the center of the pupil based on gaze angle. The weighting coefficient for gaze angle is based on eye movement in a VR system [12].

The weighting coefficient is 4.99, 5.11, 4.77, 3.84, 2.64, 1.55, 0.91, 0.5, 0.36 for 1,3,5,7,9,11,13,15,17 degree gaze angles.

E is the overall weighted distance,

$$E = \sum_{gazeangle} V_{gazeangle} * W_{gazeangle} \quad (5)$$

5. Example design parameter

The wavelength is 532nm. Single-layer design information is extracted from [1]. The effective point source location is determined by unfolding the optical system. The director equation can be found in [13] by Feng et al.

As in figure 3, the grating vector for a single layer is designed to be on Bragg for light diverting from the point source at (S_{x_0}=-53mm, S_{y_0}=27.5mm, S_{z_0}=-37mm) will be converged by the combiner at the location of the 0-degree rotated eye(P_{x_0}=27.5mm, P_{y_0} =27.5mm, P_{z_0}=0mm) in the design considered here, the combiner is 38 mm from the eye.

In the two-layer design considered in this paper, the first layer has the same grating k vector field as for the single-layer design described above.

Considering the second layer, the value α is chosen as 9 degrees.

6. Result

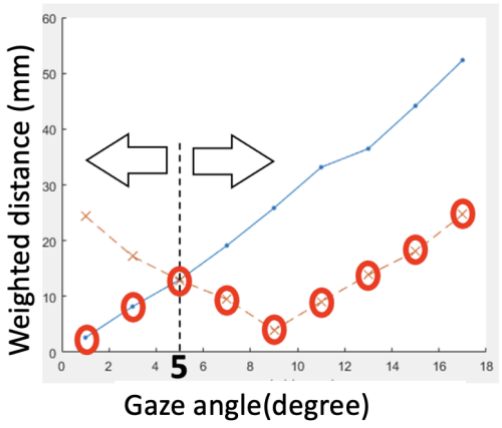

21680159, 2023, 1, Downloaded from https://sid.onlinelibrary.wiley.com/doi/10.1002/sdtp.16844 by Kent State University Standing Orders, Wiley Online Library on [03/06/2024]. See the Terms and Conditions (https://onlinelibrary.wiley.com/terms-and-conditions) on Wiley Online Library for rules of use; OA articles are governed by the applicable Creative Commons License

Figure 9. Weighted distance $V_{gazeangle}$ Vs. Gaze angle. The solid line is for the polarization state reflected by the first layer; the dashed line is for the polarization state reflected by the second layer.

The incident polarization is chosen to be the same as the layer with a lower V value(circled). When the gaze angle is <5 degrees, the incident polarization state should match the bottom layer. When the gaze angle is>5 degrees, the incident polarization state should match the top layer.

From equation (4) and equation (5), after choosing the input polarization state that has a smaller weighted distance,
R-PVH overall weighted distance for the proposed two-layer design E=207.8626mm

Improved from single layer(E=384.0426mm)=

$$\frac{384.0426 - 207.8626}{384.0426} = 45.88\%$$

7. Conclusion and discussion

In this work, we proposed an algorithm to evaluate any reflective polarization volume hologram (R-PVH) Maxwellian view design based on a weighting matrix that weighs heavier on the small field of view and gaze angle. A continuous eye movement from 0 to 17 degrees towards the ear is considered. Using the algorithm, we evaluated an example Maxwellian zone design similar to [10]. In the future, with a properly chosen, close-to-reality weighting coefficient, an optimized Maxwellian view design can be achieved for the least weighted distance to the center of the pupil for a range of gaze angles.

10. Acknowledgements

This work was funded by Reality Labs Research, Meta Platforms.

11. References

1. Jang, C., Bang, K., Li, G., & Lee, B. (2018). Holographic near-eye display with expanded eye-box. ACM Transactions on Graphics (TOG), 37, 1 - 14.

2. Lin T, Zhan T, Zou J, Fan F, Wu ST. Maxwellian near-eye display with an expanded eyebox. Opt Express. 2020 Dec 21;28(26):38616-38625. doi: 10.1364/OE.413471. PMID: 33379428.

3. Wang, L., Li, Y., Liu, S., Li, X. and Su, Y. (2021), 42.6: Maxwellian-viewing-super-multi-view near eye display using a Pancharatnam-Berry optical element. SID Symposium Digest of Technical Papers, 52: 533-536.

4. He, Z., Yin, K., Fan-Chiang, K. and Wu, S. (2021), 33-2: Student Paper: Optimized Liquid-Crystal Dammann Grating for Eyebox Expansion in Maxwellian-View Displays. SID Symposium Digest of Technical Papers, 52: 431-434. https://doi.org/10.1002/sdtp.14709

5. Xia, X., Guan, Y., Yang, F., Mei, Y., Zheng, H. and Yu, Y. (2021), 31-1: Invited Paper: Eyeglasses-Style Maxwellian-View Near-eye Display with Lens-Array-Based Holographic Optical Element. SID Symposium Digest of Technical Papers, 52: 394-397. https://doi.org/10.1002/sdtp.14699.

6. Kim S-B, Park J-H. Optical see-through Maxwellian near-to-eye display with an enlarged eyebox. Opt Lett. 2018 Feb 15;43(4):767-770. doi: 10.1364/OL.43.000767. PMID: 29443989.

7. Jang C, Bang K, Moon S, Kim J, Lee S, and Lee B. 2017. Retinal 3D: augmented reality near-eye display via pupil-tracked light field projection on retina. ACM Trans. Graph. 36, 6, Article 190 (December 2017), 13 pages.

8. Xiong J, Li Y, Li K, and Wu S-T, "Aberration-free pupil steerable Maxwellian display for augmented reality with cholesteric liquid crystal holographic lenses," Opt. Lett. 46, 1760-1763 (2021)

9.Xiong, J, Li, Y, Li, K, Wu, S-T. Aberration-free pupil steering Maxwellian display with wide-view broadband polarization converters. J Soc Inf Display. 2021; 29: 298– 304.

10. Zou, J., Li, L. and Wu, S. (2022), Gaze-Matched Pupil Steering Maxwellian-View Augmented Reality Display with Large Angle Diffractive Liquid Crystal Lenses. Adv. Photonics Res., 3: 2100362.

11. Chang C, Bang K, Wetzstein G, Lee B, Gao L. Toward the next-generation VR/AR optics: a review of holographic near-eye displays from a human-centric perspective. Optica. 2020 Nov 20;7(11):1563-1578. doi: 10.1364/OPTICA.406004. PMID: 34141829; PMCID: PMC8208705.

12.Sidenmark L and Gellersen H, 2019. Eye, Head, and Torso Coordination During Gaze Shifts in Virtual Reality. ACM Trans. Comput.-Hum. Interact. 27, 1, Article 4 (December 2019), 40 pages.

13. Feng, X., Lu, L., Lee, Y., Yaroshchuk, O., Silverstein, B. and Bos, P. (2021), 30-3: Student Paper: Polarization State Exploration and Management in Waveguide Display with Polarization Volume Gratings. SID Symposium Digest of Technical Papers, 52: 386-389.

21680159, 2023, 1, Downloaded from https://sid.onlinelibrary.wiley.com/doi/10.1002/sdtp.16844 by Kent State University Standing Orders, Wiley Online Library on [03/06/2024]. See the Terms and Conditions (https://onlinelibrary.wiley.com/terms-and-conditions) on Wiley Online Library for rules of use; OA articles are governed by the applicable Creative Commons License